Application Driven Mathematical Analysis and Statistical Classification of Multidimensional Signals.

Rick Archibald

Computer Science and Mathematics Division

ORNL

Overview

- High-order image analysis in MRI.
- Computational modeling of nano-circut architecture designed to have both logical and imaging processing functionality.
- High dimensional single trial analysis of EEG to predict fine motor neural intent .

Consortium

SWAIR
THE UNIVERSITY OF ARIZONA
Southwest Animal Imaging Resource

BARROW
Neurological Institute

Goal: *'To capitalize on the state's complementary resources in brain imaging…to help in the understanding, early detection, treatment, and prevention of Alzheimer's disease.'*

Magnetic Resonance Imaging

<u>Research Motivation:</u> Improve Sensitivity of Detecting Volume Change of Neural Structures in MRI through high order Image Reconstruction techniques.

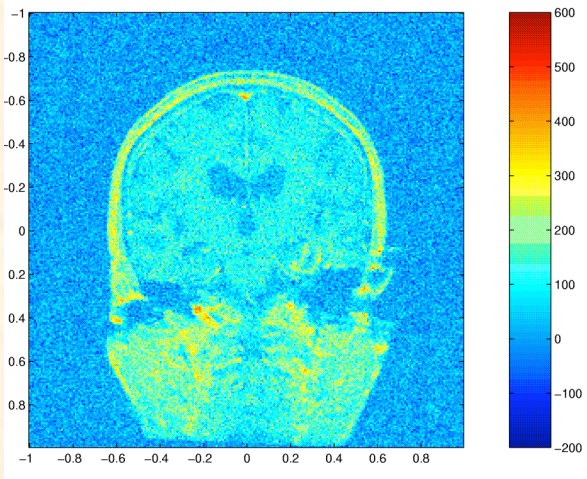

Fourier Reconstruction

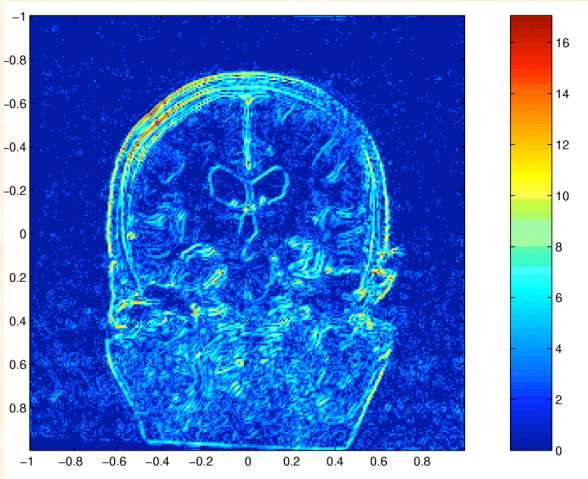

Boundary Detection

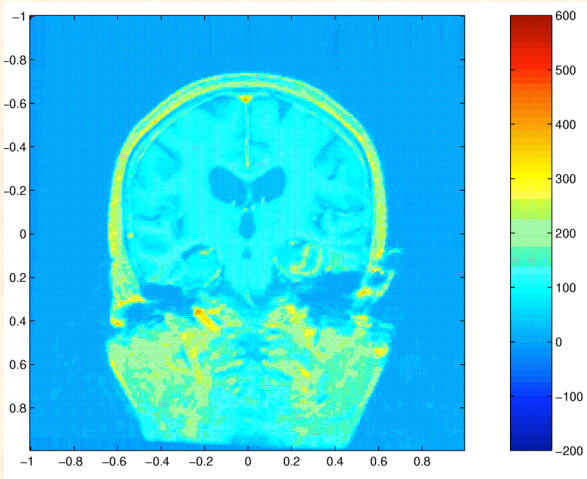

Gegenbauer Reconstruction

Fourier Reconstruction

2D Fourier Reconstruction

$$F_N(x,y) = \sum_{k=-N}^{N} \sum_{l=-N}^{N} \tilde{f}_{k,l} e^{i\pi(kx+ly)}$$

2D Fourier Coefficients

(equally spaced k-space data)

$$\tilde{f}_{k,l} = \frac{1}{4N^2 c_k c_l} \sum_{j=0}^{2N-1} \sum_{h=0}^{2N-1} f(x_j, y_h) e^{-i\pi(kx_j + ly_h)}$$

$$c_j = \begin{cases} 2 & j = \pm N \\ 1 & else \end{cases}$$

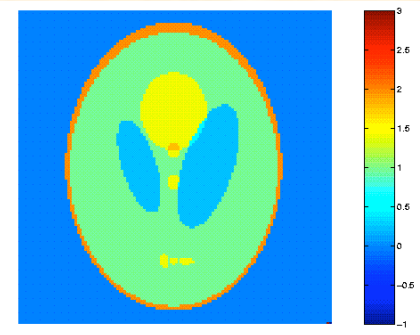

Shepp-Logan Brain Phantom

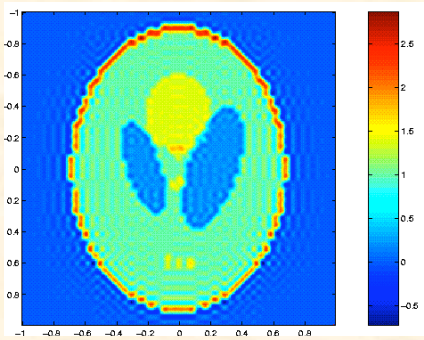

Fourier Reconstruction (128X128)

Filtered Fourier Reconstruction

2D Fourier Reconstruction

$$F_N^{\theta}(x,y) = \sum_{k=-N}^{N} \sum_{l=-N}^{N} \theta_k \theta_l \tilde{f}_{k,l} e^{i\pi(kx+ly)}$$

$$\theta_k = \theta\left(\frac{|k|}{N}\right) = e^{-\alpha\left(|k|/N\right)^p}$$

α=32

p=4

2D Fourier Coefficients

(equally spaced k-space data)

$$\tilde{f}_{k,l} = \frac{1}{4N^2 c_k c_l} \sum_{j=0}^{2N-1} \sum_{h=0}^{2N-1} f(x_j, y_h) e^{-i\pi(kx_j + ly_h)}$$

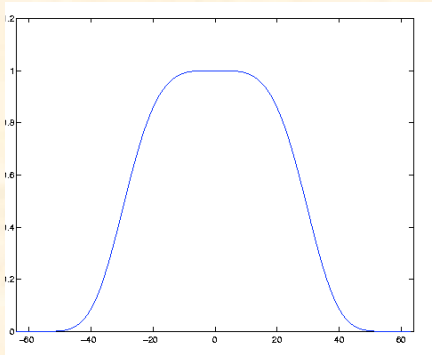

Graph of the Filter θ

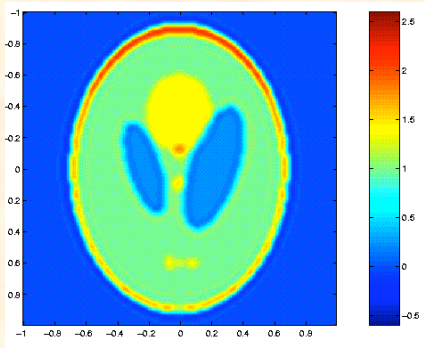

Filtered Fourier Reconstruction (128X128)

Boundary Detection

Concentration Method [Gelb and Tadmor] with Continuous Fourier Coefficients

$$K_N^{\sigma} * f(x) = i\pi \sum_{k=-N}^{N} \operatorname{sgn}(k)\sigma\left(\frac{|k|}{N}\right)\hat{f}_k e^{ik\pi x} \rightarrow [f](x)$$

Concentration factors satisfy

$$\frac{\sigma(\xi)}{\xi} \in C^2(0,1) \qquad \int_0^1 \frac{\sigma(\xi)}{\xi} d\xi = 1$$

Concentration Method with Discrete Fourier Coefficients

$$T_N^{\tau}[f](x) = i\pi \sum_{k=-N}^{N} \operatorname{sgn}(k)\tau\left(\frac{|k|}{N + 1/2}\right)\tilde{f}_k e^{ik\pi x} \rightarrow [f](x)$$

Where the Discrete Concentration factors satisfy

$$\tau(\xi) = \sigma(\xi)\frac{2\sin(\xi\pi)}{\xi\pi}$$

Gegenbauer Reconstruction

The Gegenbauer reconstruction method [Gottlieb, et.al.] recovers piecewise smooth functions with spectral accuracy *up to* the edges in each smooth interval.

- Given f(x), an piecewise smooth function in [-1,1] that is analytic in a sub-interval [a,b].
- Define the local variable η is defied such that x(η)=εη+δ such that

$$\varepsilon = \frac{b-a}{2}, \qquad \text{and} \qquad \delta = \frac{b+a}{2}.$$

- The Gegenbauer coefficients:

$$f_m^\lambda(\eta(x)) = \sum_{l=0}^{m} \hat{f}_{l,\varepsilon}^\lambda C_l^\lambda(\eta), \quad -1 \le \eta \le 1,$$

where

$$\hat{f}_{l,\varepsilon}^\lambda = \frac{1}{h_l^\lambda} \int_{-1}^{1} \left(1-\eta^2\right)^{\lambda-\frac{1}{2}} C_l^\lambda(\eta) f(x(\eta)) d\eta.$$

- Convergence is exponential with the max norm in [a,b] for m,λ~εN.

Gegenbauer Method Continued

It is possible to approximate the Gegenbauer coefficients using the truncated Fourier reconstruction and still maintain spectral accuracy *up to* the edges in each smooth interval.

- Define the approximation to the Gegenbauer coefficients

$$\hat{g}_{l,\varepsilon}^{\lambda} = \frac{1}{h_l^{\lambda}} \int_{-1}^{1} \left(1-\eta^2\right)^{\lambda-\frac{1}{2}} C_l^{\lambda}(\eta) f_N(x(\eta)) d\eta.$$

- The new partial sum approximation becomes

$$f_m^{\lambda}(\eta(x)) = \sum_{l=0}^{m} \tilde{g}_{l,\varepsilon}^{\lambda} C_l^{\lambda}(\eta), \quad -1 \le \eta \le 1.$$

- Convergence remains exponential with the max norm in [a,b] for m,λ~εN.

Shepp-Logan Phantom Example

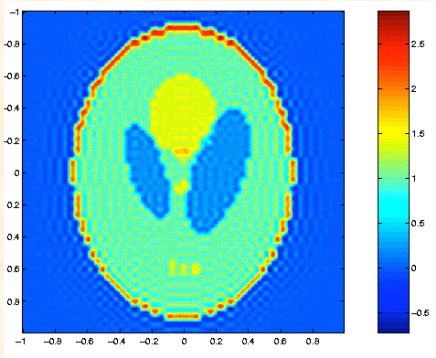

Fourier Reconstruction (128X128)

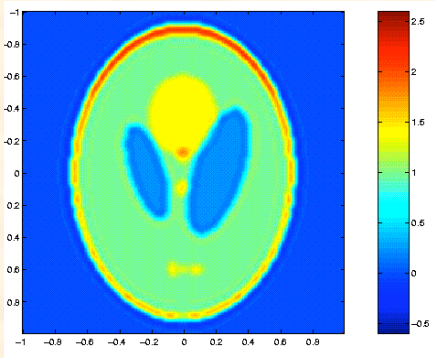

Filtered Fourier Reconstruction (128X128)

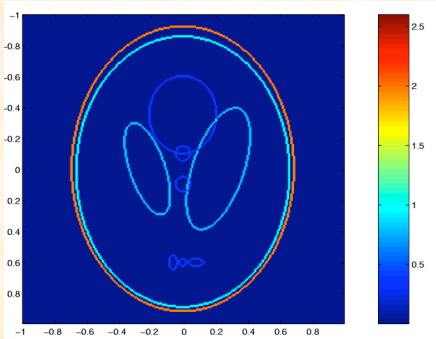

Boundary Detection Using Minimization Method

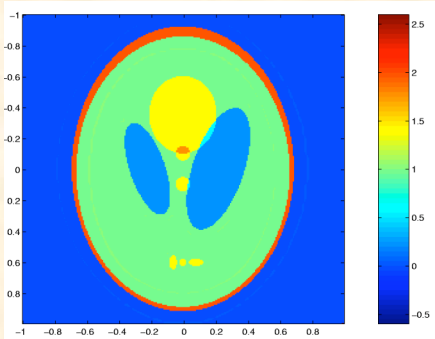

Gegenbauer Reconstruction using the Fourier Reconstruction with $m=\lambda=4$.

Artificial Noise Reduction

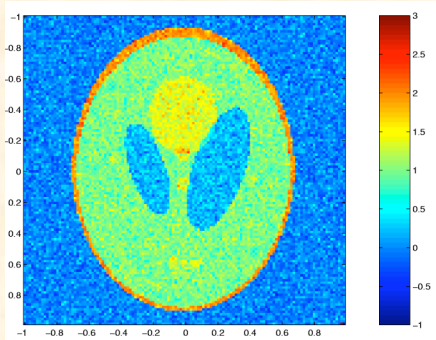

Fourier Reconstruction (128X128)

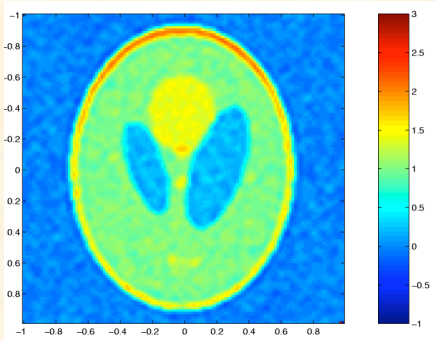

Filtered Fourier Reconstruction

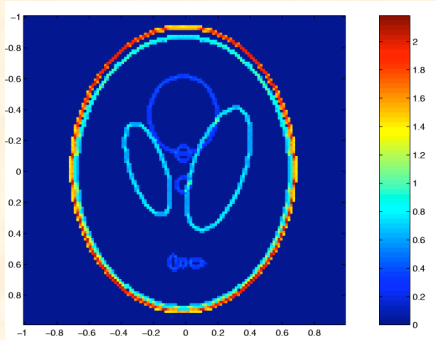

Boundary Detection Using Minimization Method and Noise Reduction.

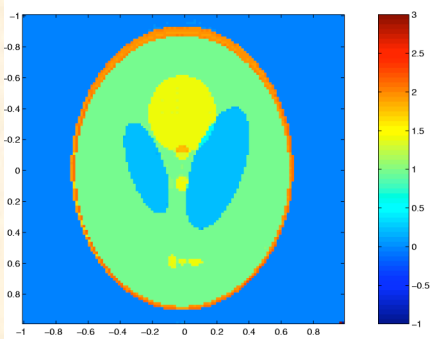

Gegenbauer Reconstruction using the Fourier Reconstruction with m=λ=4.

Gegenbauer Preprocessing

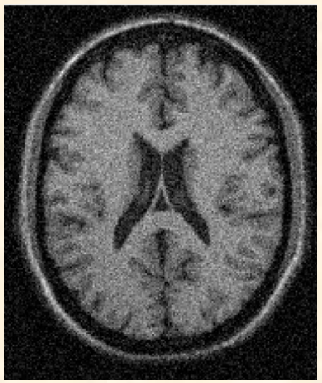

MR Image

SPM Segmentation

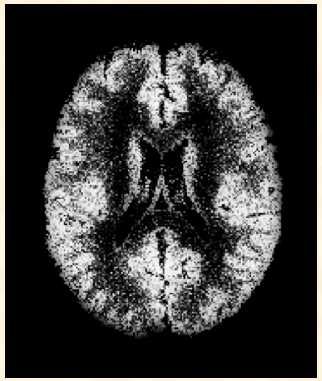

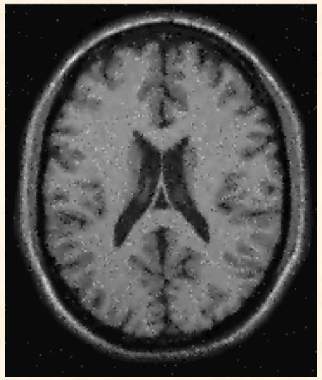

Gegenbauer Reconstruction

SPM Segmentation

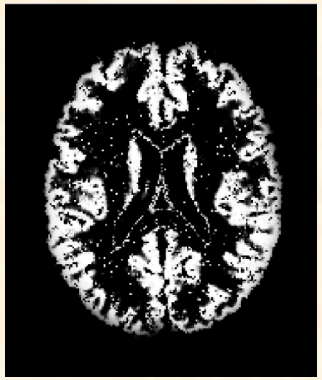

Gray Matter Probability Maps

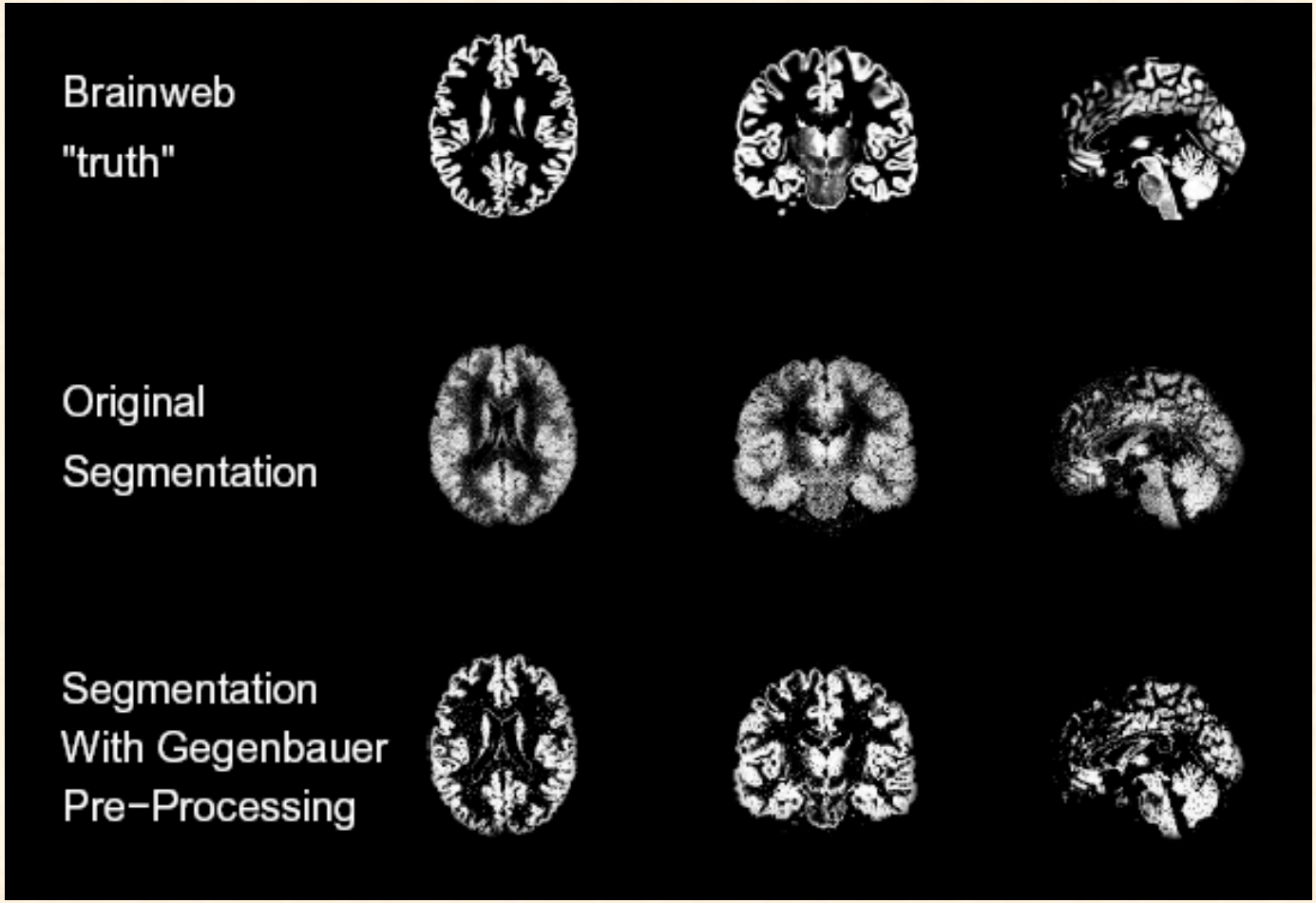

Gray matter segmented probability maps for the original and Gegenbauer image reconstruction of a particular randomly generated MNI digital brain phantom with 9% level of noise and 40% INU.

Brain Extraction

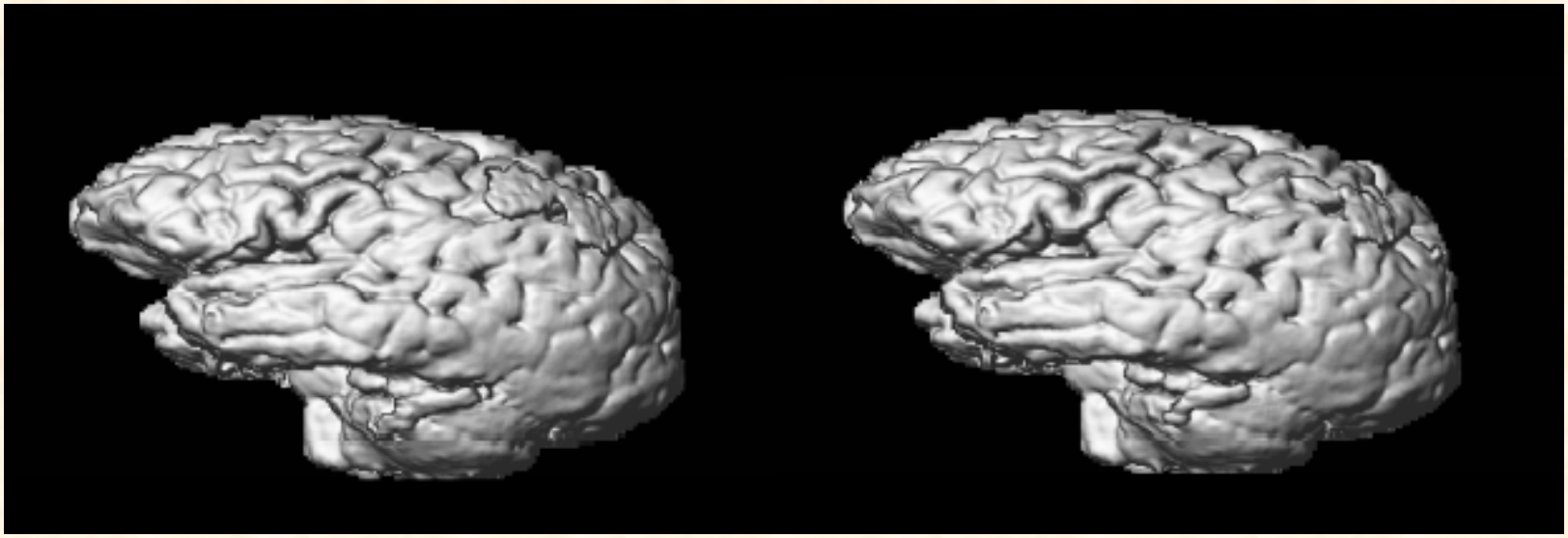

SPM Brain Extraction

SPM Brain Extraction With Gegenbauer Pre-Processing

High Dimensional Segmentation

The Weibull E-SD field segmentation method [Hu, et.al.] generates for each data point an ordered pair representing the local expectation and standard deviation. Segmentation occurs by clustering regions in the E-SD field -- a valid method under the assumption that homogeneous structures can be characterized by similar local expectancy and variance.

$$p(v) = \frac{a}{b}\left(\frac{v - v_0}{b}\right)^{a-1} \exp\left[-\left(\frac{v - v_0}{b}\right)^{a}\right]$$

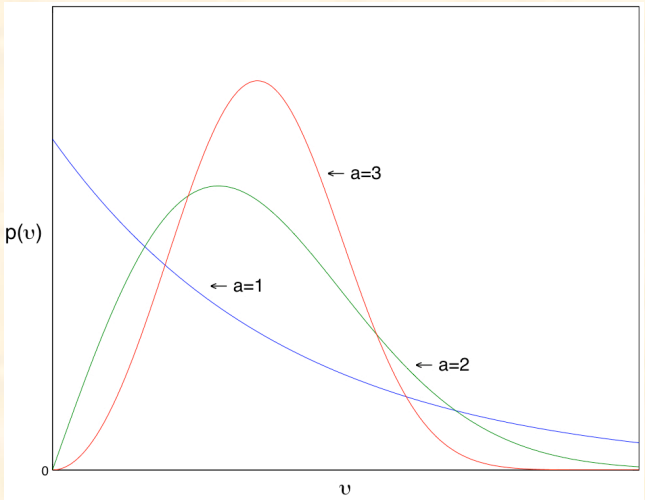

Weibull probability density function (pdf).
Note: Approximates Possion pdf for a=1, Rayleigh pdf for a=2, and Gaussian pdf for a=3.

Control Problem

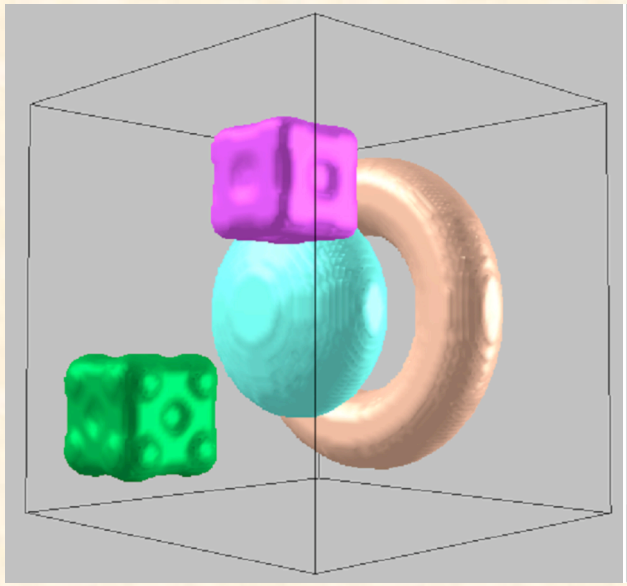

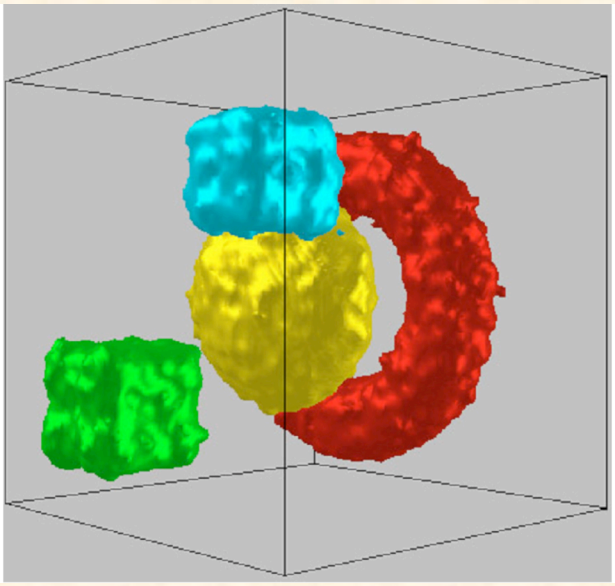

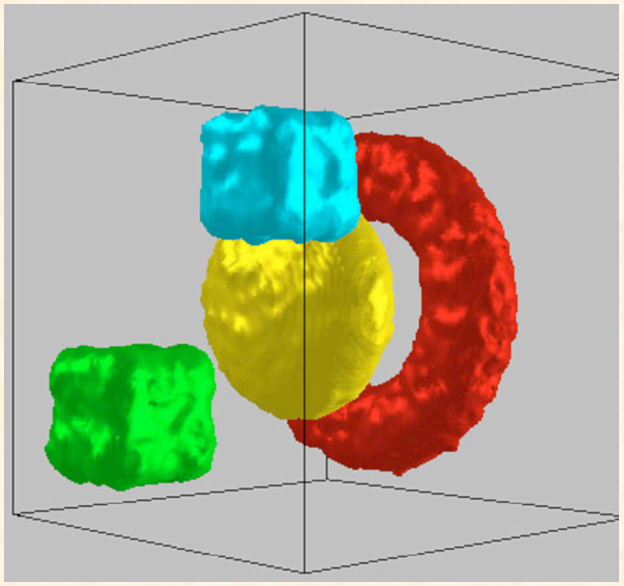

Simulated Volume Data

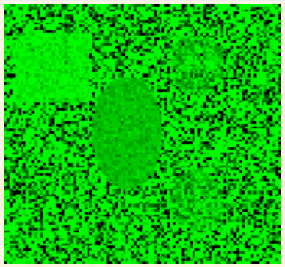

E-SD Field Segmentation

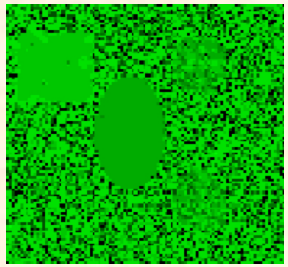

Gegenbauer Preprocessing

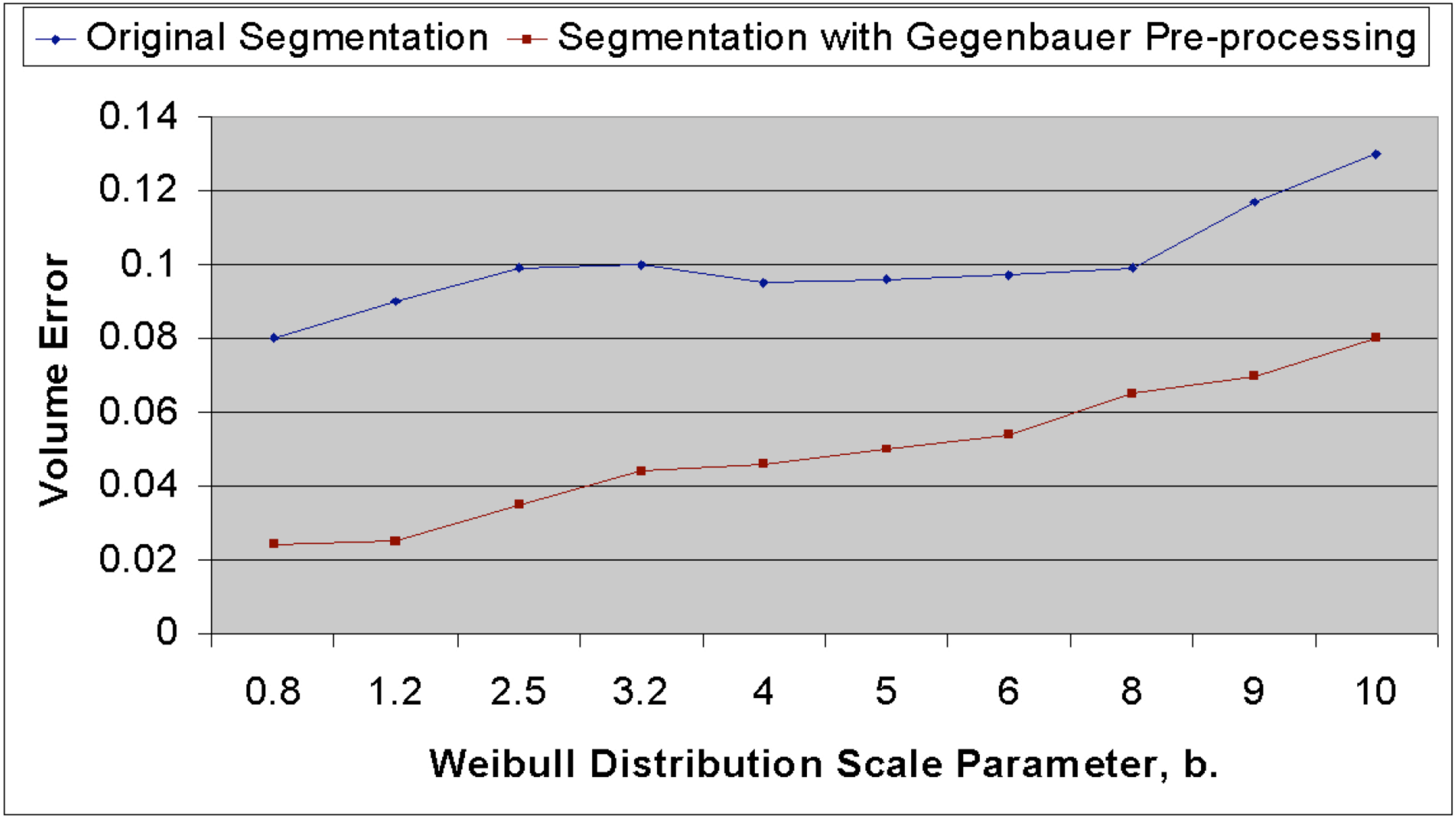
Original Segmentation
Segmentation with Gegenbauer Pre-processing
Volume Error
0.14
0.12
0.1
0.08
0.06
0.04
0.02
0
0.8
1.2
2.5
3.2
4
5
6
8
9
10
Weibull Distribution Scale Parameter, b.

Small Animal MRI Segmentation

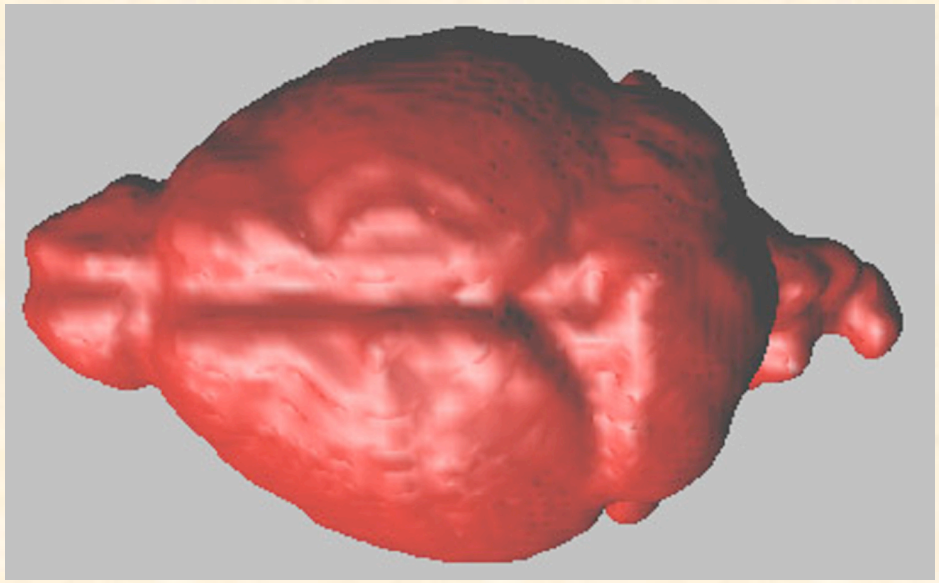

Original Segmentation (Top)

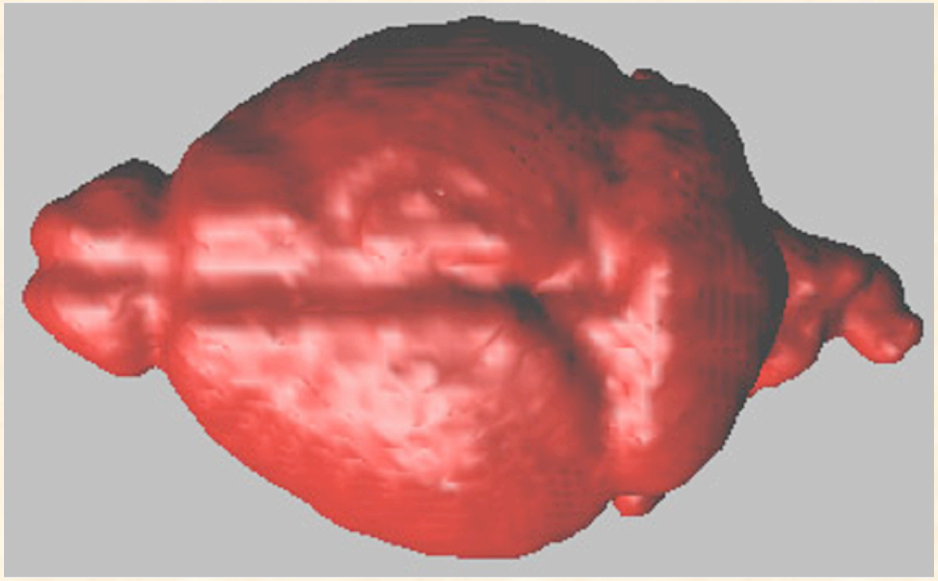

Gegenbauer Preprocessing

Majority of the 10% volumetric difference occurs near boundaries

Small Animal MRI Segmentation

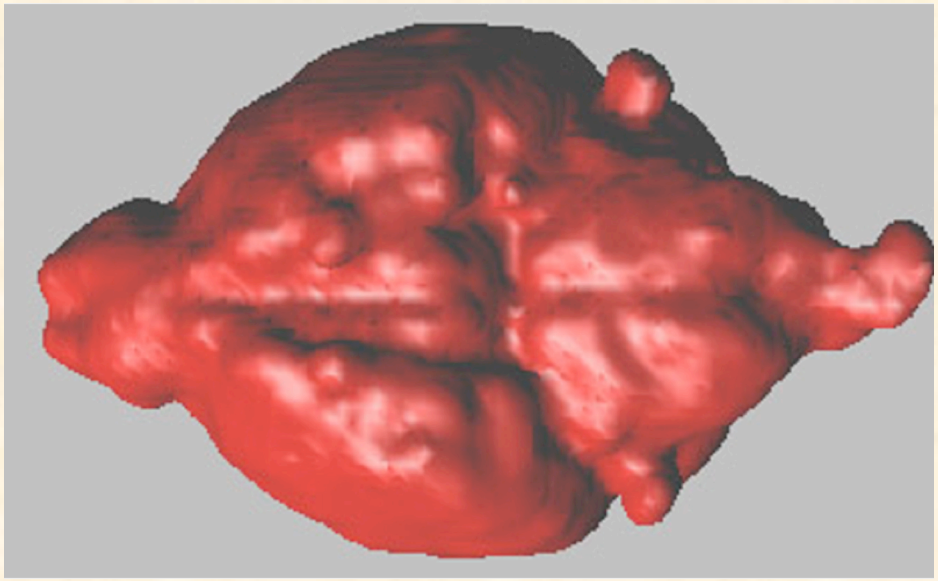

Original Segmentation (Bottom)

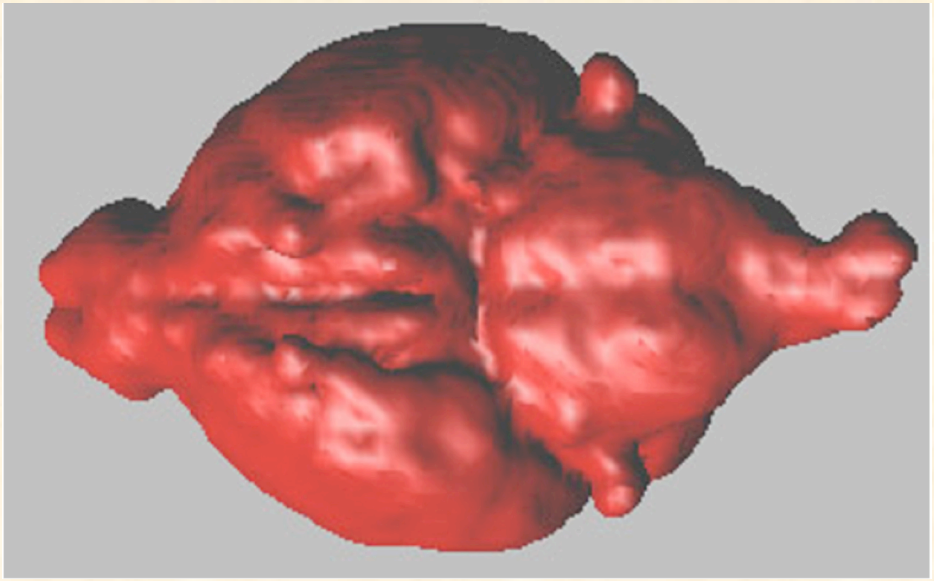

Gegenbauer Preprocessing

Majority of the 10% volumetric difference occurs near boundaries

boundaries of segmented homogeneous objects are more accurate, and the representation of homogeneous objects is better constrained in the E-SD field. Additionally, the combination of these methods is a viable approach for segmentation of volumetric data due to their low computational cost and robust nature in the presence of various types of noise.

ACKNOWLEDGMENTS

The work of these authors was supported in part by the Center for System Science and Engineering Research at Arizona State University (R. Archibald and A. Gelb), the Arizona Center for Alzheimer's Disease Research (G. Farin), the US Defense Advanced Research Projects Agency grant No MDA 972-00-1-0027 (J. Hu and G. Farin), NSF grant No DMS01-07428 (A. Gelb), NSF grant No EAR0222327 (A. Gelb), and No IIS-998016 (G. Farin). The authors would like to thank Southwest Small Animal Imaging Resource and PRISM for providing the data and computing resources.

REFERENCES

[1] R. Archibald, K. Chen, A. Gelb, and R. Renaut, "Improving Tissue Segmentation of Human Brain MRI Through Pre-Processing by the Gegenbauer Reconstruction Method," *NeuroImage*, in press.

[2] R. Archibald and A. Gelb, "A Method to Reduce the Gibbs Ringing Artifact in MRI Scans While Keeping Tissue Boundary Integrity," *IEEE Transactions of Medical Imaging*, vol. **21**, pp. 305-319, 2002.

[3] R. Archibald and A. Gelb, "Reducing the effects of noise in boundary detection," *Journal of Scientific Computing*, vol. **17**, pp. 167-180, 2002.

[4] C. Chesnaud, P. Refregier, and V. Boulet, "Statistical Region Snake-

Rick Archibald received the BSc degree in honors physics and M.Sc in applied mathematics from University of Alberta, Canada, in 1996 and 1998 respectively. He received the PhD degree in mathematics from Arizona State University in 2002. Presently he is working as a post-doctorate at the Center for System Science and Engineering Research at Arizona State University. His current research interests includes spectral image reconstruction, biological modelling, boundary detection and stochastic problems.

Jiuxiang Hu received the BS, MS, and PhD degrees in mathematics from Huazhong Normal University in 1988, Huazhong University of Science and Technology, Wuhan, China, in 1991, and Lanzhou University, Lanzhou, China in 1994, respectively. He has been an assistant research scientist in the Bioengineering Department and PRISM lab at Arizona State University since 2000. Since receiving the PhD degree, he was a postdoctoral fellow from 1995 to 1996 and then joined the Department of Computer Science, Huazhong University of Science and Technology, where he was promoted to associate professor in 1997. His research interests include computer graphics, visualization, image processing, and expert systems. He has developed and implemented methods to segment biomedical volume data sets, including image statistical modelling and segmentation techniques with application to structural and quantitative analysis of 3D images.

Generalized Edge Detection

<u>Research Motivation:</u> Develop an edge detection method with portability to a broad range of scientific applications.

- Can be applied to any irregular data in any domain
- Independent of any specific shape of discontinuities in both the univariate and multivariate case.
- Easy to implement numerically -- cost effective.
- High order method.

Formulation in Multiple Dimensions

Suppose that a piecewise smooth function is sampled on a finite number of points

$$S = \{x_1, x_2, \ldots, x_N\} \subset \Omega \subset R^d.$$

The coefficients of the edge detector at the point $x \in \Omega$ is the solution to the linear system

$$\sum_{x_j \in S_x} c_j(x) p_i(x_j) = \sum_{|\alpha|_1 = m} p^{(\alpha)}(x) \quad \alpha \in Z_+^d,$$

Where p_i, $i=1,\ldots,m_d$, is a polynomial basis of order m. Note:

$$m_d = \binom{m+d}{d}, \; |\alpha|_1 = \sum_{j=1}^{d} \alpha_j, \;\; S_x = \{x_1, x_2, \ldots, x_{m_d}\}.$$

The edge detector $L_m f$ is defined as

$$L_m f(x) = \frac{1}{q_{m,d}(x)} \sum_{x_j \in S_x} c_j(x) f(x_j) = [f](x) + O\left(h^{m_x}(x)\right).$$

Here [f](x) is the jump function, h(x) is a density function and the normalization factor depends upon the order m, dimension d, and the local set S_x and is defined as

$$q_{m,d}(x) = \sum_{x_j \in S_x^+} c_j(x).$$

Discontinuities in the γth derivative can be detected by adding the following restriction

$$\sum_{x_j \in S_x^+} c_j(x) \overline{p}_i(x_j) = \sum_{|\alpha|_1 = \gamma} \overline{p}^{(\alpha)}(x) \quad \alpha \in Z_+^d,$$

and modifying the normalization factor to become

$$q_{m,d}(x) = \sum_{x_j \in S_x^+} c_j(x) \frac{(x_j - x)^\gamma}{\gamma!}.$$

Example: Scattered Data in 1D.

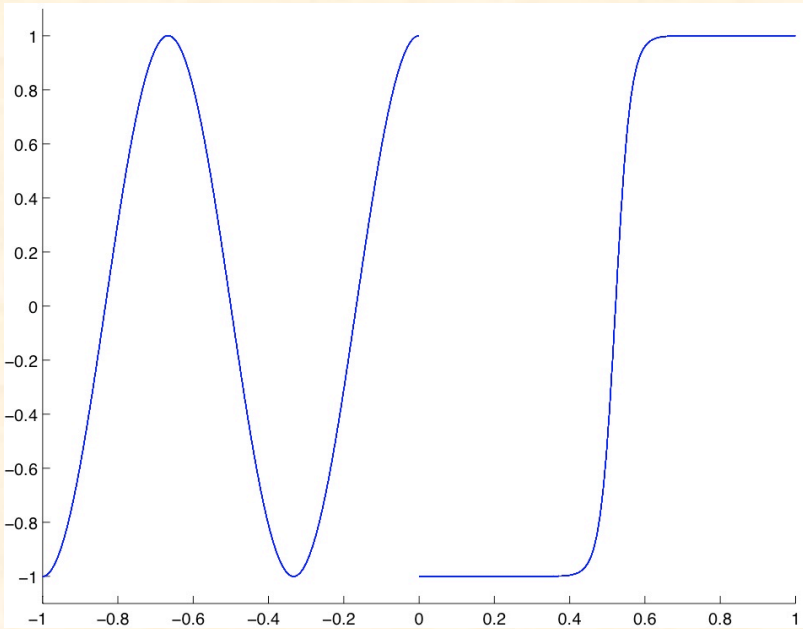

Function

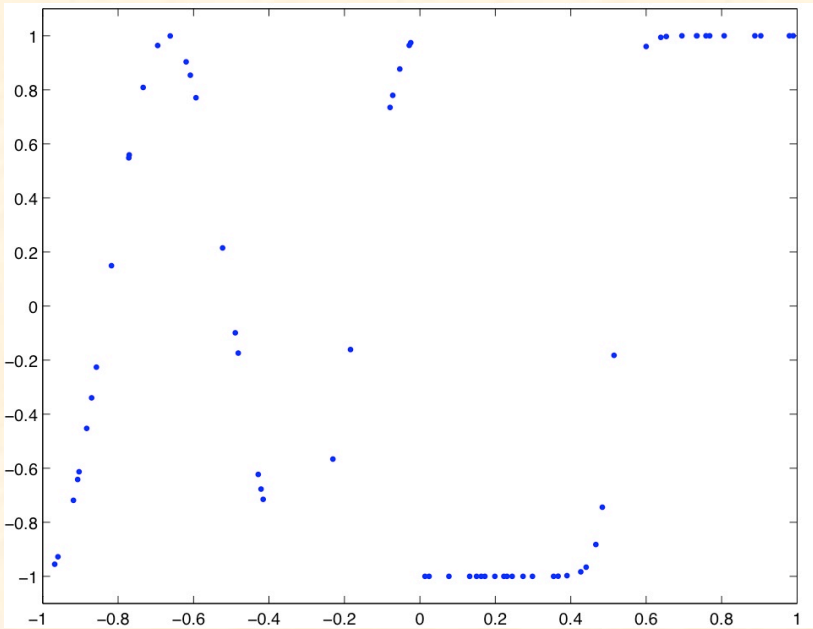

Sampling (N=64)

$$f(x) = \begin{cases} \cos(3\pi x) & -1 \le x \le 0, \\ \dfrac{2}{1+3e^{-50x+25}} - 1 & 0 < x \le 1. \end{cases}$$

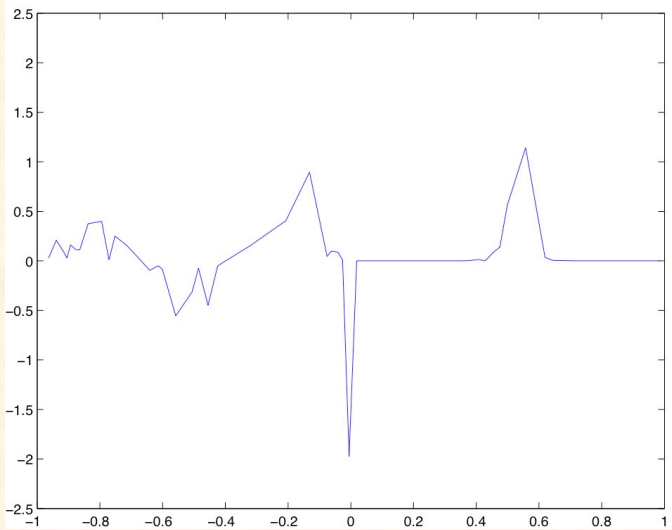

$L_1 f(x)$

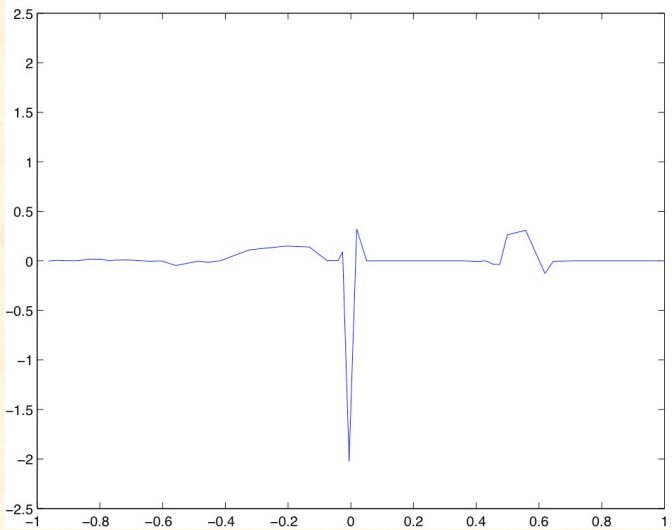

$L_3 f(x)$

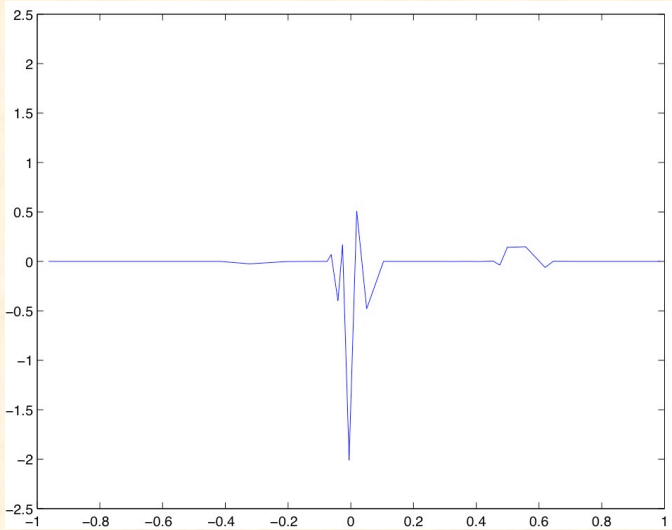

$L_6 f(x)$

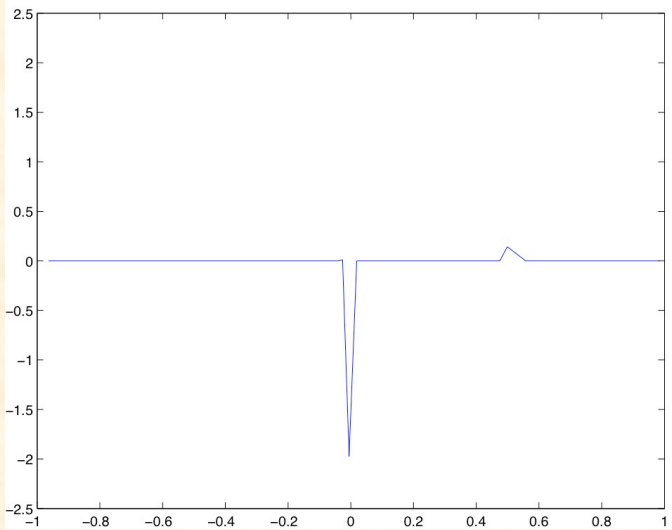

Minmod of $L_m f(x)$

Example: Scattered Data in 2D

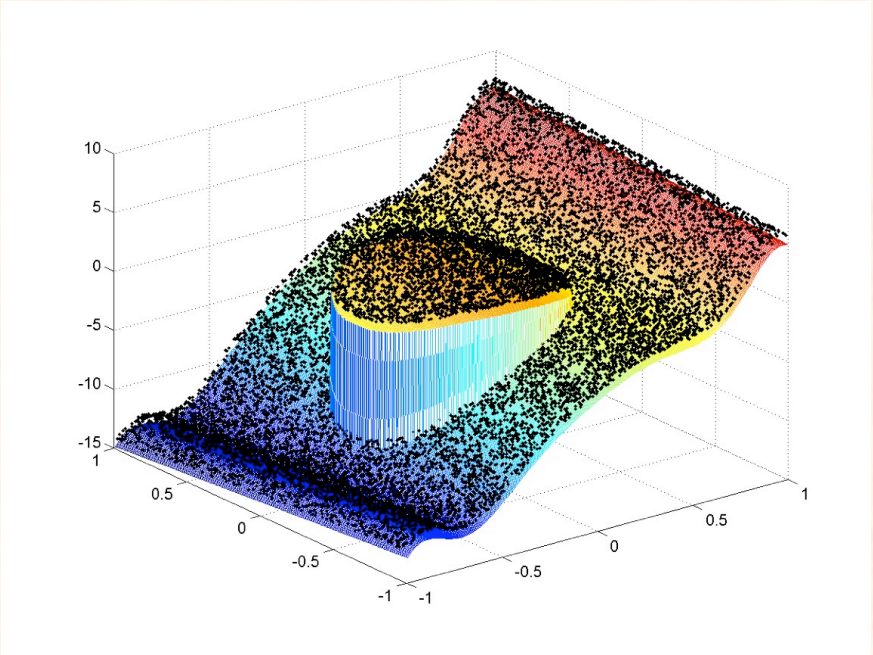

Function and Sampling (N=128X128)

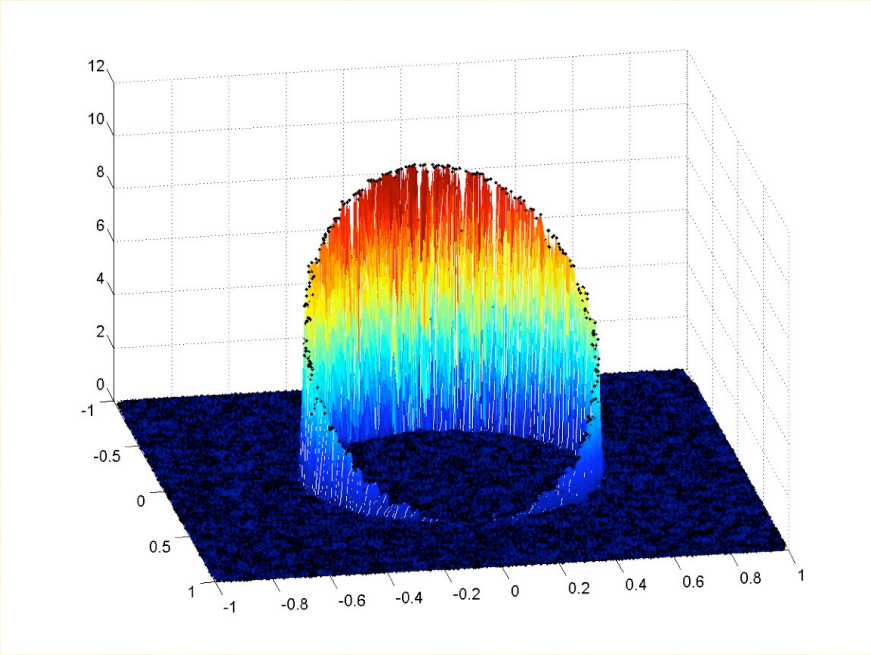

Minmod Boundary Detection

$$f(x,y)=\begin{cases} xy+\cos\left(2\pi x^2\right)-\sin\left(2\pi x^2\right) & x^2+y^2\le\frac{1}{4}, \\ 10x-5+xy+\cos\left(2\pi x^2\right)-\sin\left(2\pi x^2\right) & x^2+y^2>\frac{1}{4}. \end{cases}$$

Example: Singularity Detection

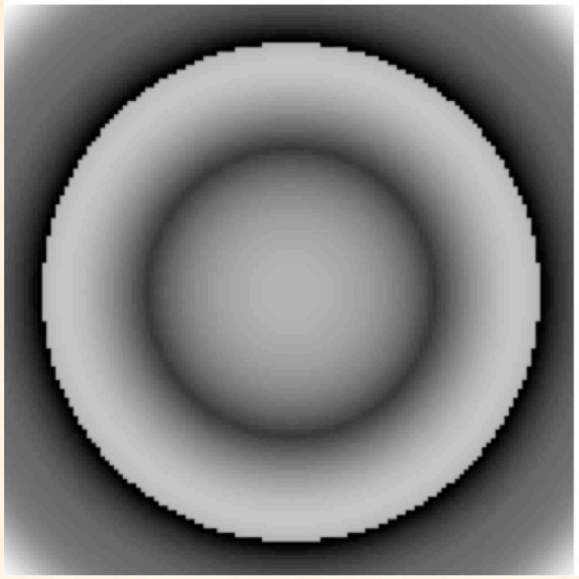

Function

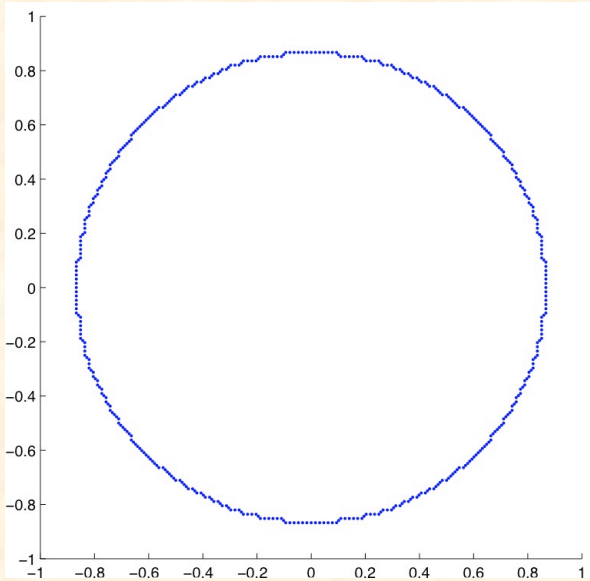

Minmod on $L_m f(x)$ with $\gamma=0$.

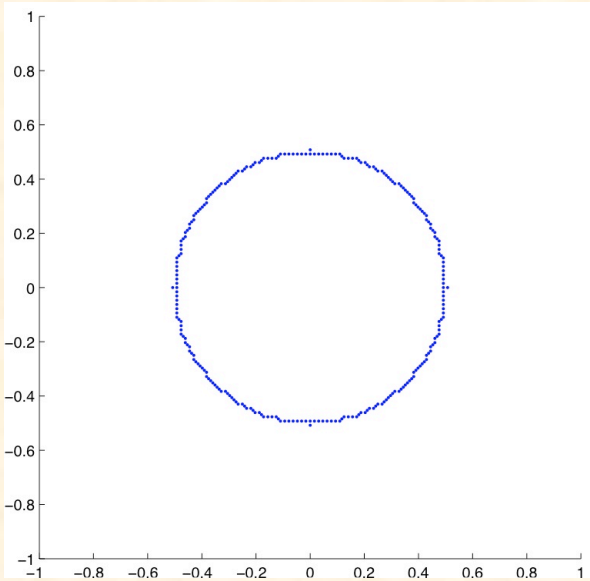

Minmod on $L_m f(x)$ with $\gamma=1$.

$$f(r)=\begin{cases} -r\sin\left(\dfrac{\pi r^2}{2}\right) & r\le -\dfrac{1}{3}, \\ \left|\sin(2\pi r)\right| & -\dfrac{1}{3}<r<\dfrac{1}{3}, \quad r=\dfrac{4x^2+4y^2-1}{4}. \\ 2r-1-\dfrac{1}{6}\sin(3\pi r) & r\ge\dfrac{1}{3}, \end{cases}$$

Center on Functional Engineered Nano Architectonics (FENA)

Next generation of nanoscale semiconductor technology:

- interfaces of new nanosystems.
- biological and molecular functions.
- paradigms of information processing and sensing.
    - Locally connected and highly parallel forms of information processing similar to those in the brain.
- New nanostructured materials.

Weakly Connected Neural Networks (WCNN)

Consider the WWCN as described by the dynamical system:

$$\dot{X}_i = F_i(X_i, \lambda) + \varepsilon G_i(X_1, \ldots, X_N, \lambda, \rho, \varepsilon), \quad i = 1, \ldots, N.$$

The fundamental theorem of WCNN states that the equilibrium point ρ must be a near a bifurcation point in order for the network dynamics to be nontrivial [Hoppensteadt and Izhikevich].

WCNN

- Canonical models near equilibrium points are obtained through the use center manifold reduction, change of variables, and rescaling or averaging.
  - The dynamics of many different nano-systems can be distilled to an equivalent network of oscillators.
    - Rate coupled network of oscillators that have saddle-node dynamics is proven to be capable of basic logical operations and the image processing function of boundary detection

Architecture of the Network

Consider the NXM networked oscillators, where the phase is described in terms of its natural oscillation and phase deviation as

$$\theta_{i,j} = \Omega_{i,j} t + \phi_{i,j},$$

for i=1,2,…,N and j=1,2,…,M. Here the phase deviation dynamics of the ith, j^{th} oscillator has saddle-node dynamics on an invariant circle (SNIC),

$$\left(1 + \varepsilon C(\phi)\right)\dot{\phi}_{i,j} = \left(1 + \cos\phi_{i,j}\right)a_{i,j} + \left(1 - \cos\phi_{i,j}\right)b_{i,j}.$$

Here $a_{i,j}$ and $b_{i,j}$ is the inputs to the ith, jth oscillator (naturally coupled to the nearest neighbors), ε is a small parameter, and C(Φ) represents the coupling of the ith, jth oscillator to its neighborhood.

Example: OR Logical Operation

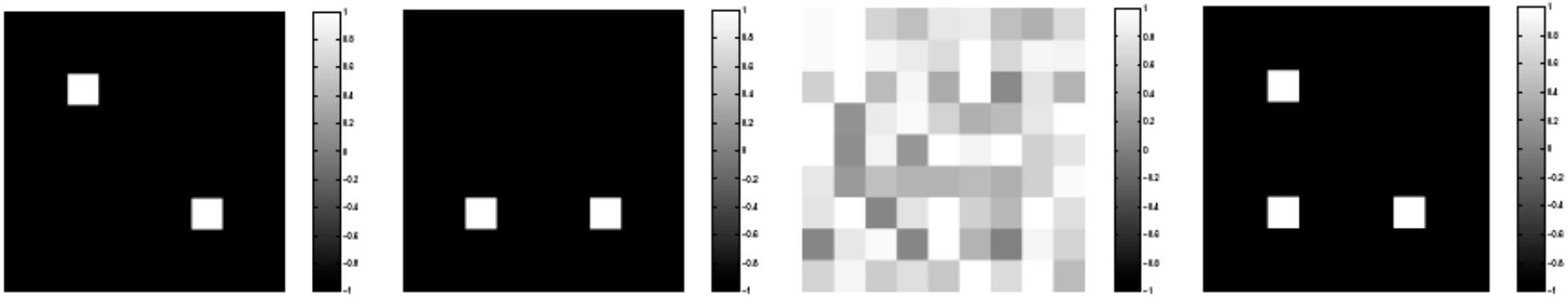

Binary images (a) U and (b) V. (c) Initial conditions. (d) The sine of the steady state solution of equation of the rate coupled network, with

$$a_{i,j} = U_{i,j} + V_{i,j} + 1 \quad and \quad b_{i,j} = -a_{i,j}.$$

Here the rate coupling is random with N=M=9 and ε =0.1.

Example: Boundary Detection

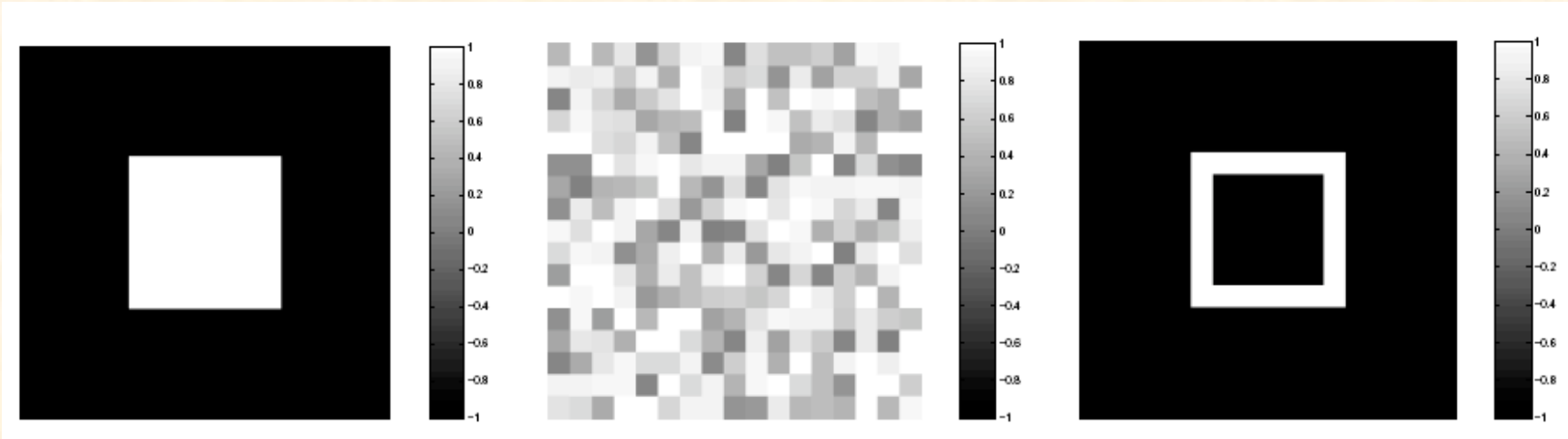

Binary images (a) U and (b) Initial conditions. (c) The sine of the steady state solution of equation of the rate coupled network, with

$$a_{i,j} = 8U_{i,j} - \sum_{\substack{0<|i-k|\le 1 \\ 0<|j-l|\le 1}} U_{k,l} - \frac{1}{2} \quad and \quad b_{i,j} = -a_{i,j}\,.$$

Here the rate coupling is random with N=M=18 and ε =0.1.

Brain Computer Interface

Michael Nagle, 25, is the first patient in a clinical trial that seeks to proce brain-comper interfaces can return function to paralyzed people.

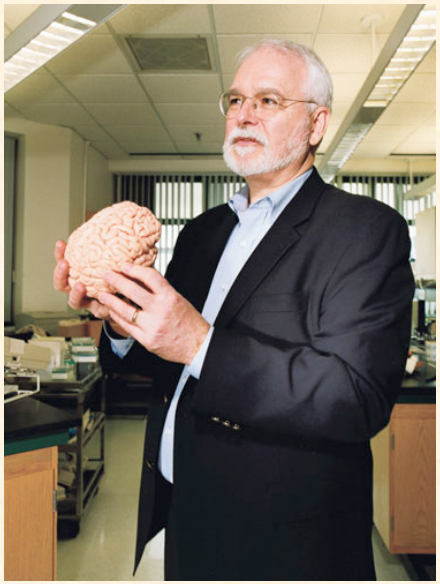

Professor John Donohue, head of neuroscience at Brown University, the founder of Cvberkinetics and creator of BrainGate.

Single Trial EEG

Objective: Explore the predictive power of single trial analysis of EEG in the context of leftward and rightward directed hand movements.

Methods: The dynamics of cortical electrical activity obtained from 14 right-handed adult volunteers was analyzed using both broad-band and independent component (IC) techniques. Classification rates of left from right movements were determined by the leave-one-out, cross-validation method, with a support vector machine, on EEG and independent components (ICs).

Why EEG

	EEG	MEG	PET	fMRI
Physiological signal	Electric Potential	Magnetic Potential	Oxygen or glucose metabolism in brain	Oxygen or glucose metabolism in brain
Temporal resolution	Very high (<1ms)	Very high (<1ms)	Low (seconds – minutes)	Low/medium (seconds)
Costs	Low	High	High	High
Application	Non invasive	Non invasive	Mildly invasive	Non invasive
Portability	High	Low	Low	Low

EEG Setup and Standard Analysis

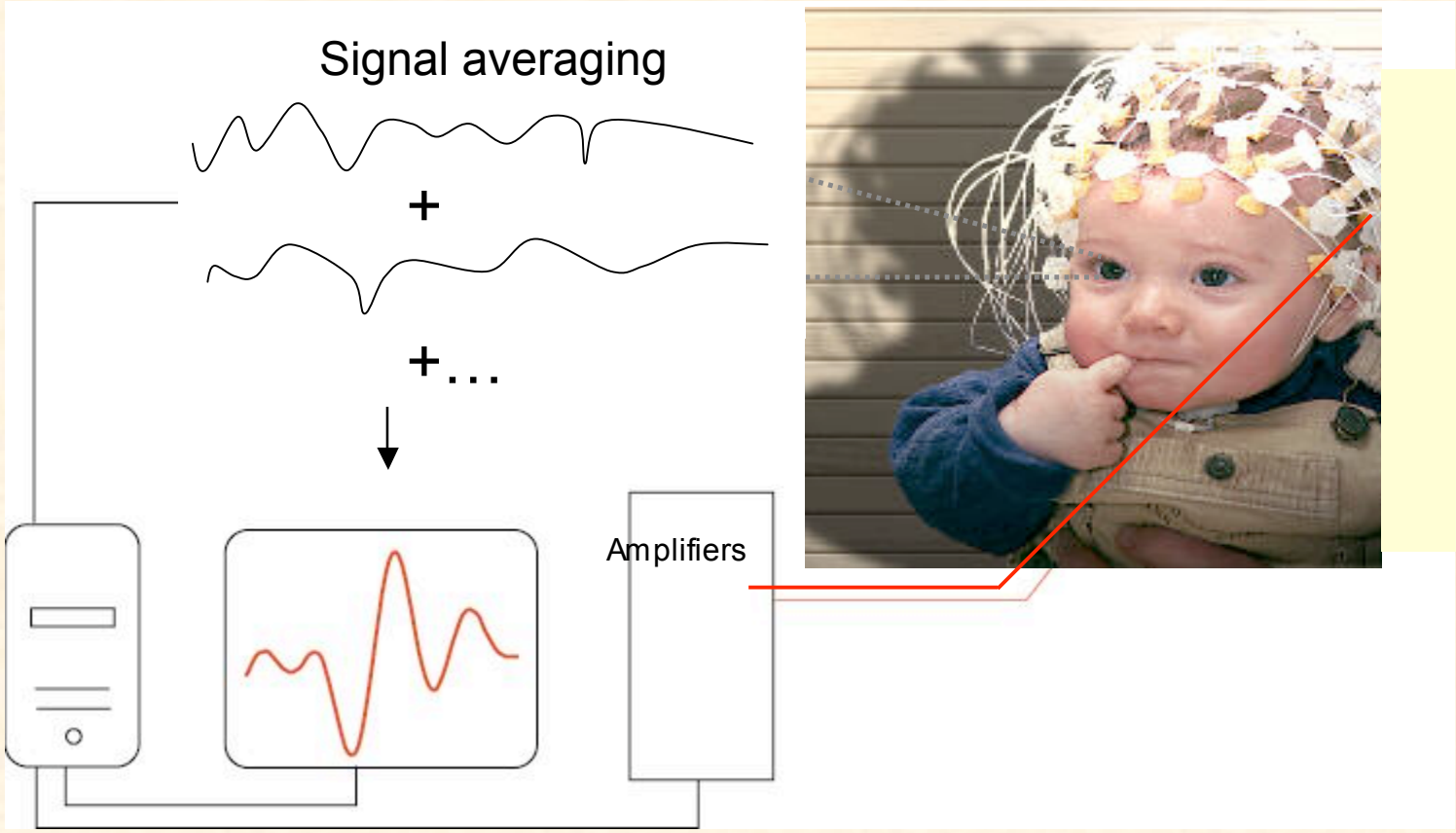

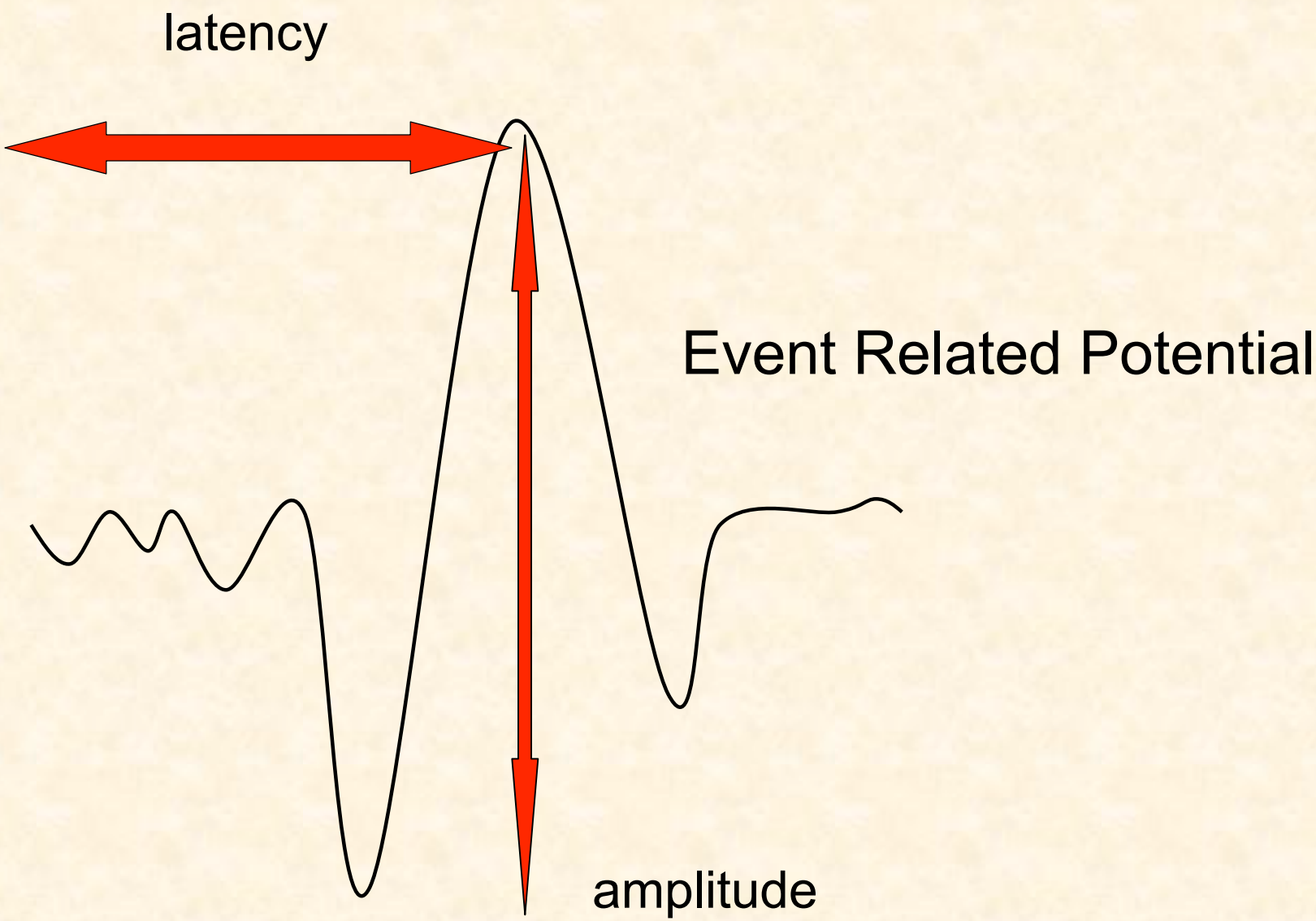
latency
Event Related Potential
amplitude

Independent Component Analysis

Let x(t) be an n-dimensional vector of sensor signals produced by the ***linear*** mixing of s(t), and ***unknown*** n-dimensional vector of ***independent*** sources,

$$x(t) = As(t).$$

Here the unknown mixing matrix is square and assumed to be ***invertible***. This problem is also referred to as blind source separation. The particular ICA algorithm chosen for this study was SOBI [Cardoso] since it exploits the temporal data structure by minimizing the correlation between sources at different time delays. Every ICA algorithm determines the unmixing matrix up to scaling and permutation:

$$W = DPA^{-}.$$

ICA example

$$s(t) = \begin{pmatrix} \cos\left(\frac{13\pi t}{500}\right) \\ sign\left\{\cos\left(\frac{\pi t}{25}\right)\right\} \\ \xi(t) \end{pmatrix} + \zeta(t),$$

$$x(t) = \begin{pmatrix} 0.0149 & -2.0788 & -1.5583 \\ 0.2187 & 0.1129 & 0.6374 \\ 1.7132 & -1.0865 & -0.4046 \end{pmatrix} s(t)$$

$$s(t) = Wx(t).$$

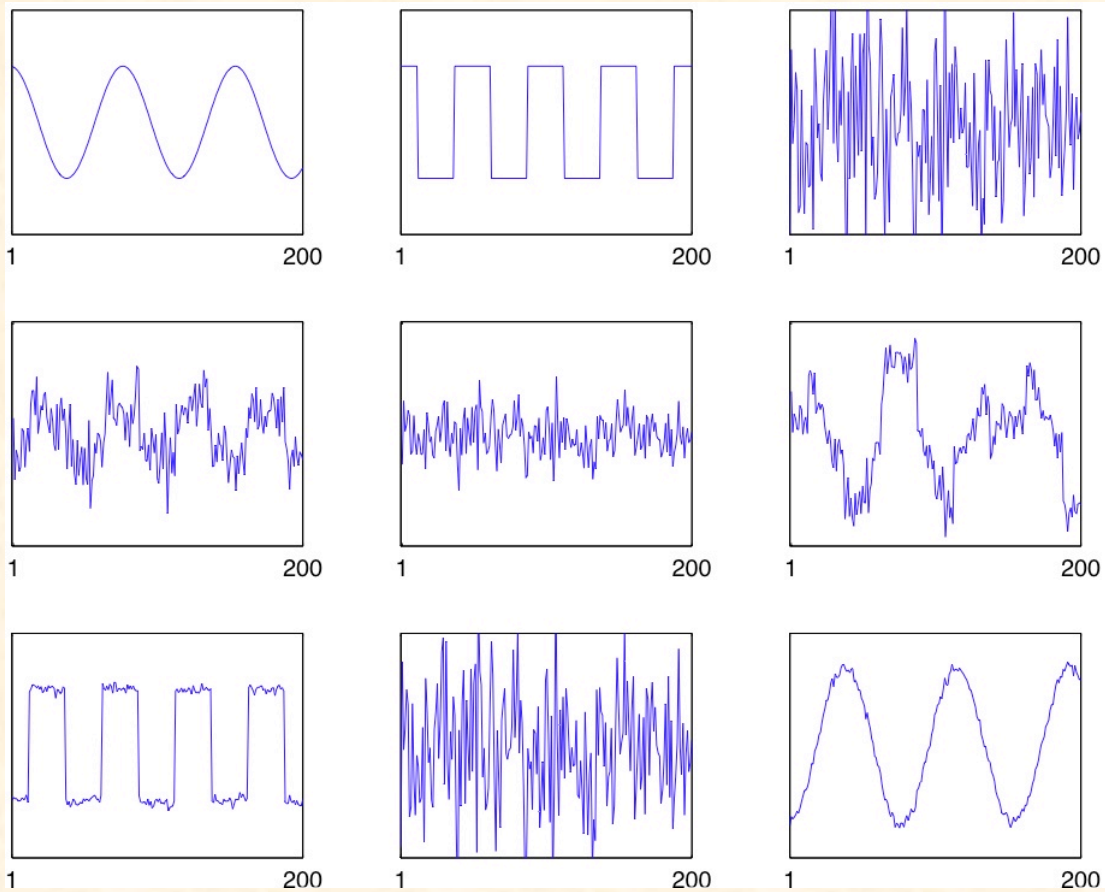

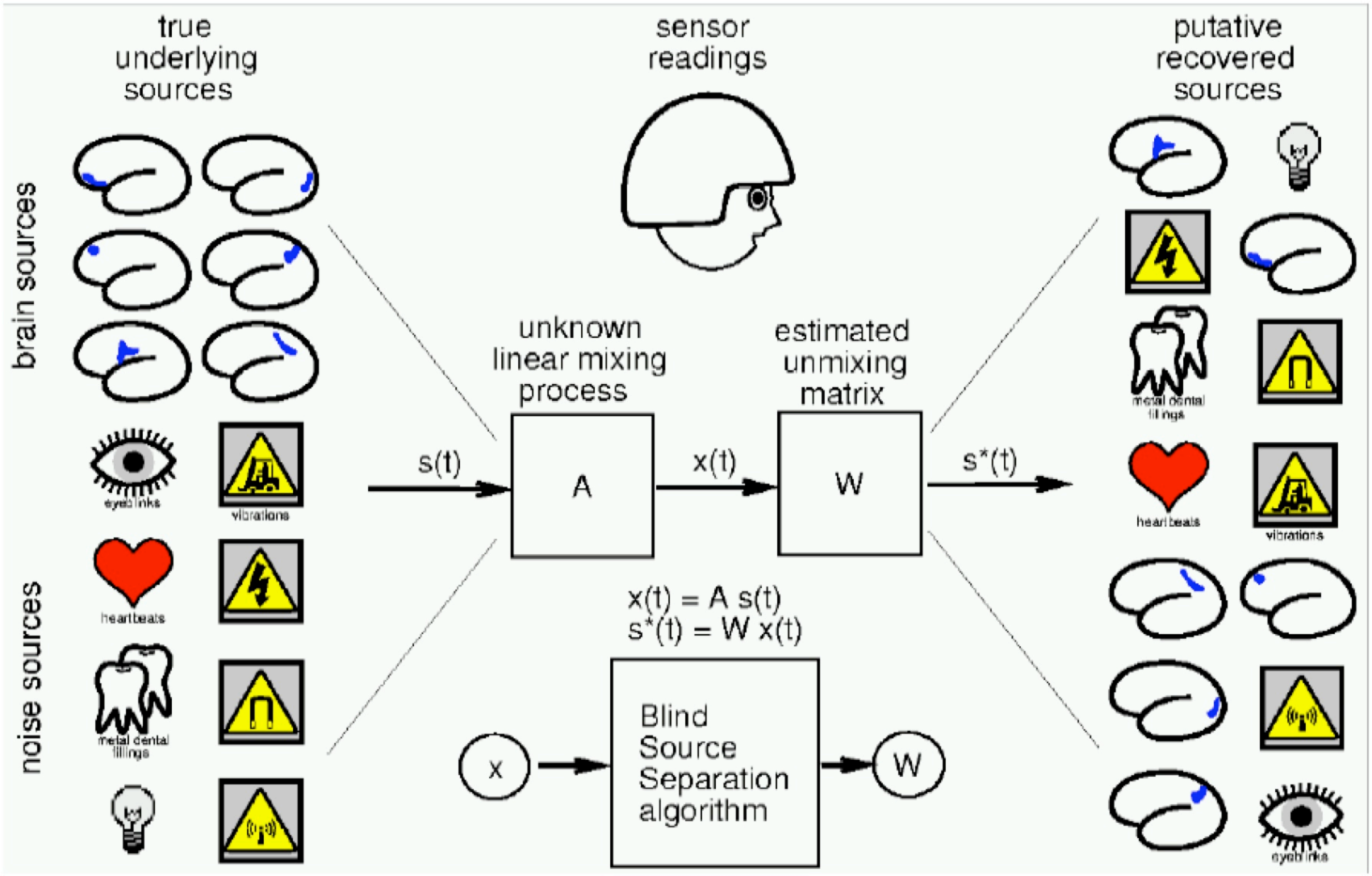
true
underlying
sources
sensor
readings
putative
recovered
sources
brain sources
noise sources
eyeblinks
vibrations
heartbeats
metal dental
fillings
unknown
linear mixing
process
estimated
unmixing
matrix
s(t)
A
x(t)
W
s*(t)
x(t) = A s(t)
s*(t) = W x(t)
x
Blind
Source
Separation
algorithm
W

ICA Summary

- Inverse problem ill-posed [Helmholtz], and sources estimation is possible only by imposing major restrictions [Darvas, et.al.]
- ICA has been demonstrated to separate EEG and MEG data into physiologivally and functionally distinct sources [Makeig, et.al.], [Jung, et.al.]
- ICA can remove ocular and other artifiacts from EEG and MEG data [Zhou and Gotman]

Support Vector Machines

Given the training set ($\mathbf{x}_i \in R^N, y_i \in \pm 1$) for i=1,..,m, the training of a support vector machine [Vapnik] leads to the following quadratic optimization problem:

$$\min: \quad W(\alpha) = -\sum_{i=1}^{m} \alpha_i + \frac{1}{2} \sum_{i=1}^{m} \sum_{j=1}^{m} y_i y_j \alpha_i \alpha_j k(x_i, x_j)$$

$$with: \quad \sum_{i=1}^{m} y_i \alpha_i = 0$$

$$\forall i: 0 \le \alpha_i \le C$$

Decision function becomes:

$$f(x) = \operatorname{sgn}\left(\sum_{i=1}^{m} y_i \alpha_i k(x, x_i) + b \right)$$

$$b = \underset{0<\alpha_j<C}{Avg} \left\{ y_j - \sum_{i=1}^{m} y_i \alpha_i k(x_j, x_i) \right\}.$$

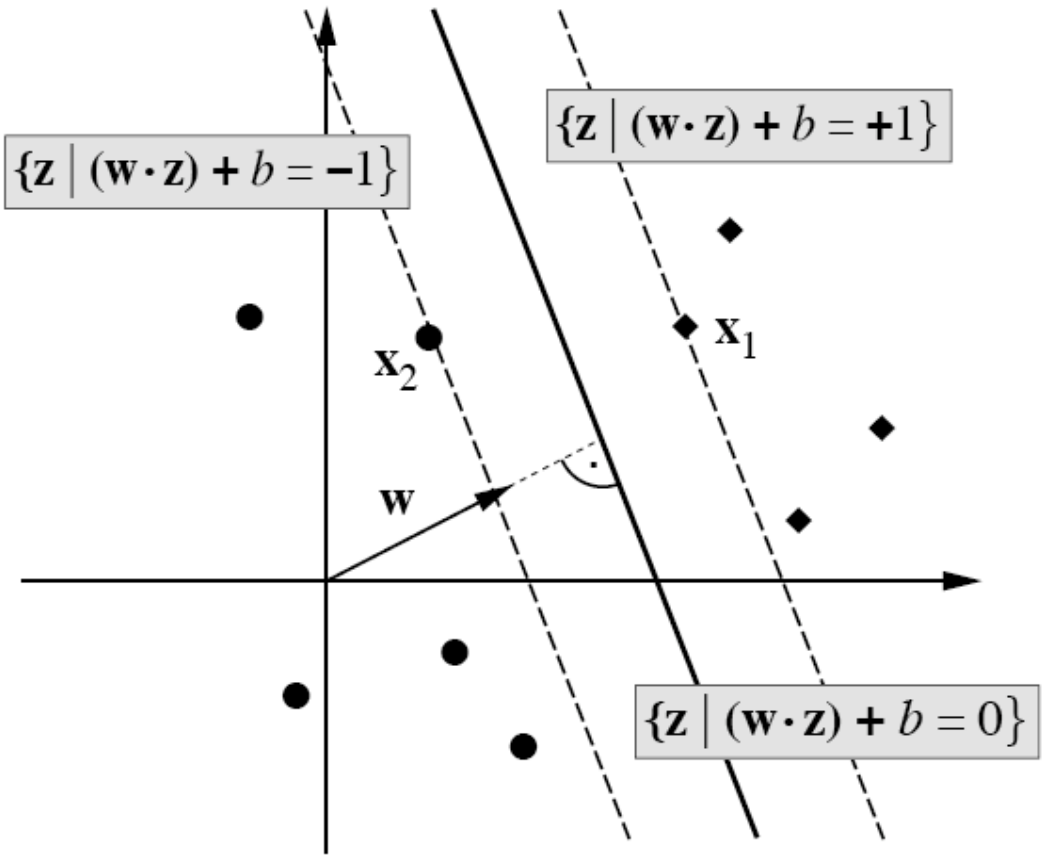

Note:

$$(\mathbf{w}\cdot\mathbf{z}_1) + b = +1$$
$$(\mathbf{w}\cdot\mathbf{z}_2) + b = -1$$

$$\Rightarrow \quad (\mathbf{w}\cdot(\mathbf{z}_1 - \mathbf{z}_2)) = 2$$

$$\Rightarrow \left(\frac{\mathbf{w}}{\|\mathbf{w}\|}\cdot(\mathbf{z}_1 - \mathbf{z}_2)\right) = \frac{2}{\|\mathbf{w}\|}$$

$$\min: \quad \|w\|$$
$$with: \quad |(w\cdot z) + b| \geq 1$$

Ideal hyperplane will be perpendicular to the shortest line connecting the convex haul of each class.

Nonlinear SVM

- To allow for more generalized decision surface, nonlinearly transform input vectors into a high-dimensional feature space by a map Φ.
- Computational costs are significantly reduced by a suitable kernel such that

$$\Phi(x) \cdot \Phi(x_i) = k(x, x_i)$$

i.e. consider the second order polynomial map

$$\Phi(x) : (x_1, x_2) \mapsto (x_1^2, x_2^2, x_1 x_2)$$

$$\Phi(x) \cdot \Phi(y) = (x \cdot y)^2$$

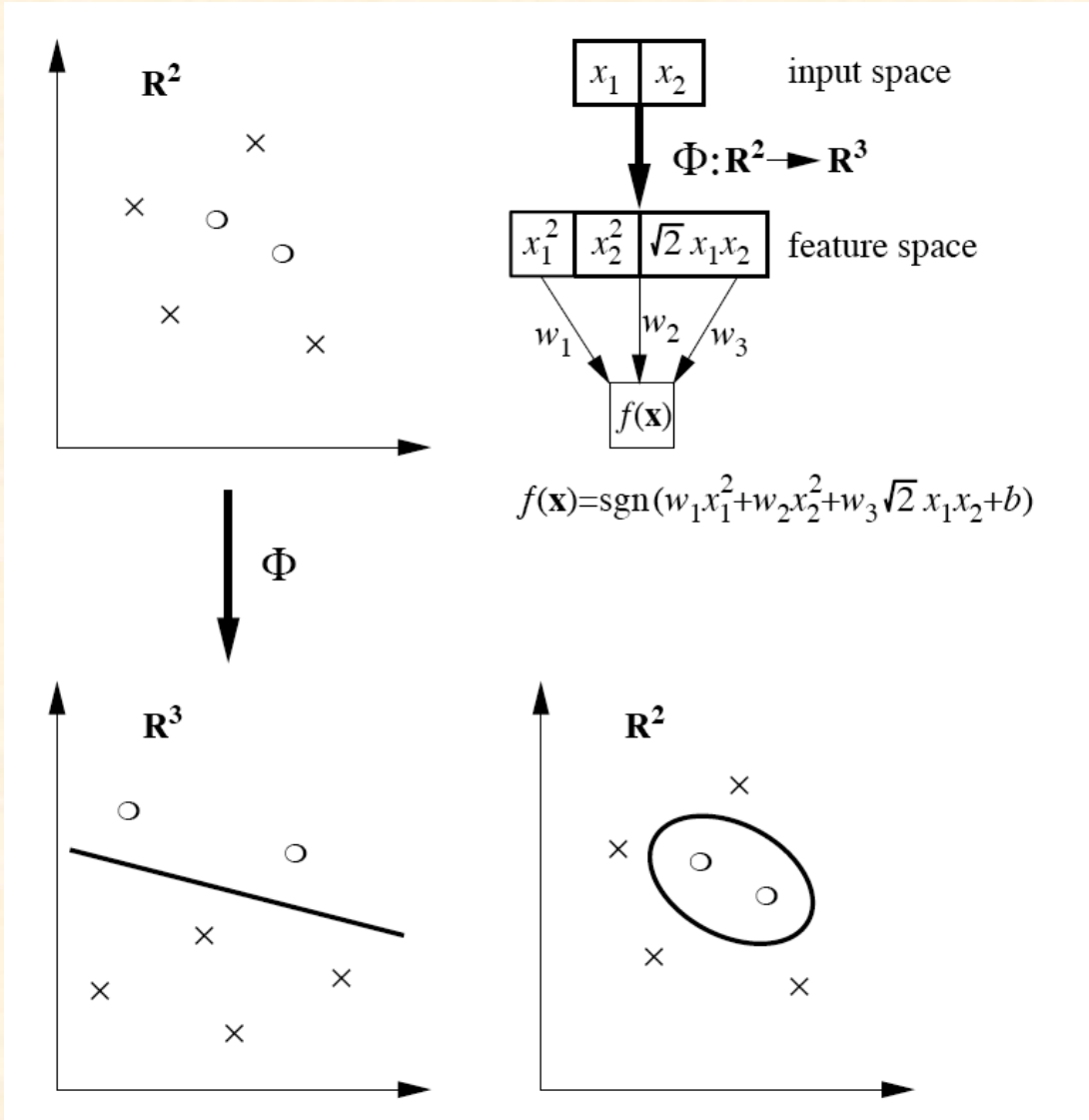
R2
x1 x2
input space
Φ:R2→R3
x1^2 x2^2 √2 x1x2
feature space
w1 w2 w3
f(x)
f(x)=sgn(w1x1^2+w2x2^2+w3√2 x1x2+b)
Φ
R3
R2

Typical Kernels

Polynomial

$$k(x, x_i) = (x \cdot x_i)^d$$

Radial Basis Function

$$k(x, x_i) = \exp\left(-\|x - x_i\|^2 / 2 \right)$$

Neural Network

$$k(x, x_i) = \tanh\left(\kappa(x \cdot x_i) + \Theta\right).$$

EEG Experiment

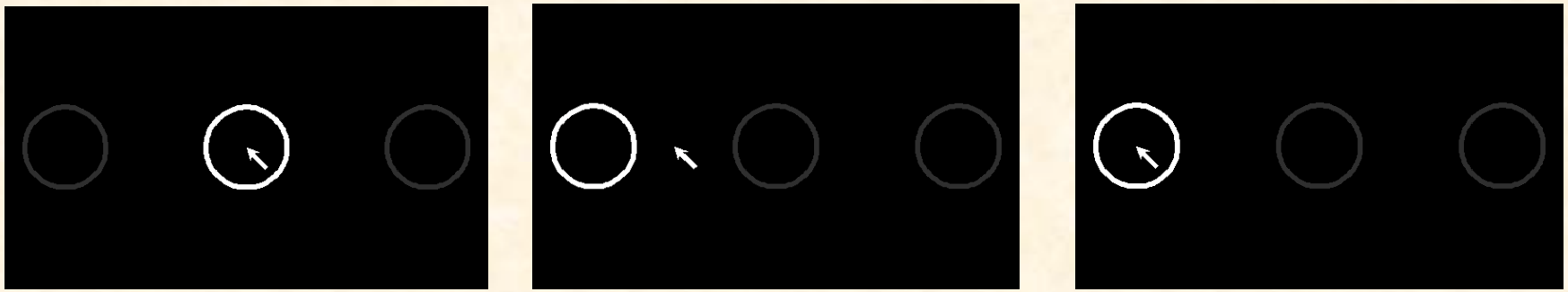

Captions of the video display for one particular trail in which the target is moved from center to left. Trial begins with the subject waiting for the cue and ends with the subject acquiring the target.

Eye Movements

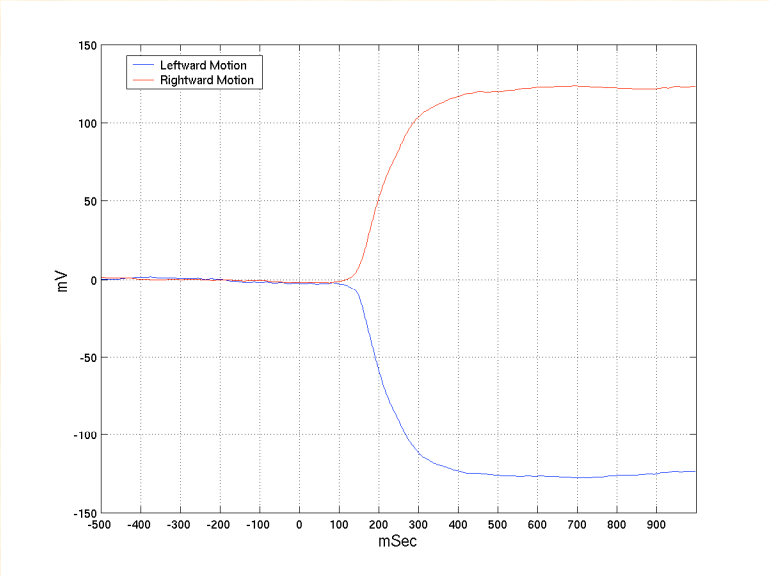

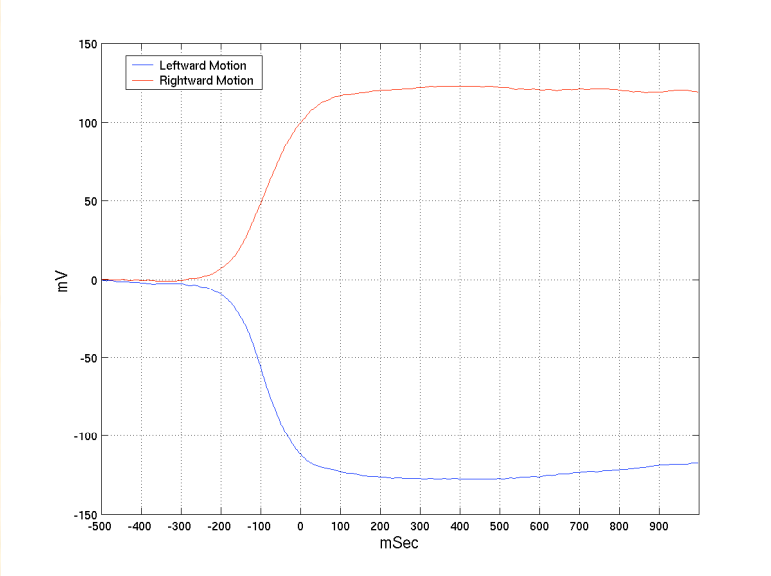

Grand average of leftward versus rightward movement trials of EEG data recorded the HEOG channel for both (a) stimulus and (b) movement locking.

EEG Cap Array

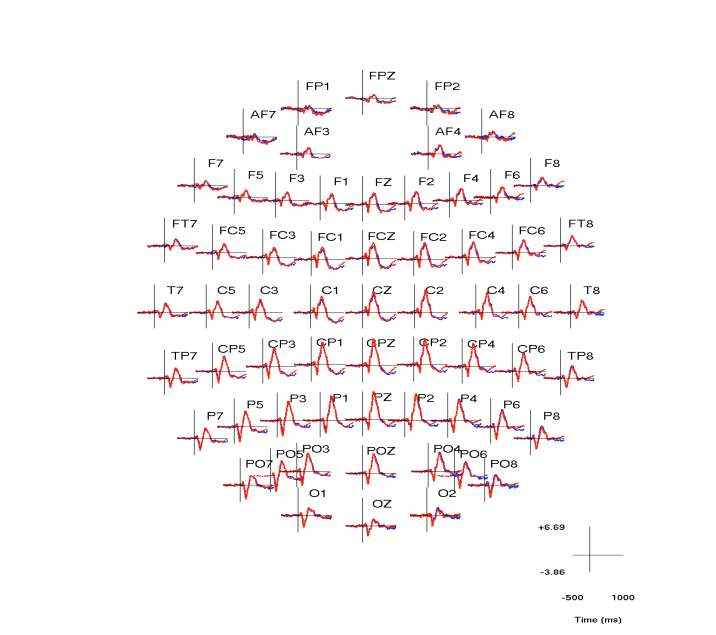

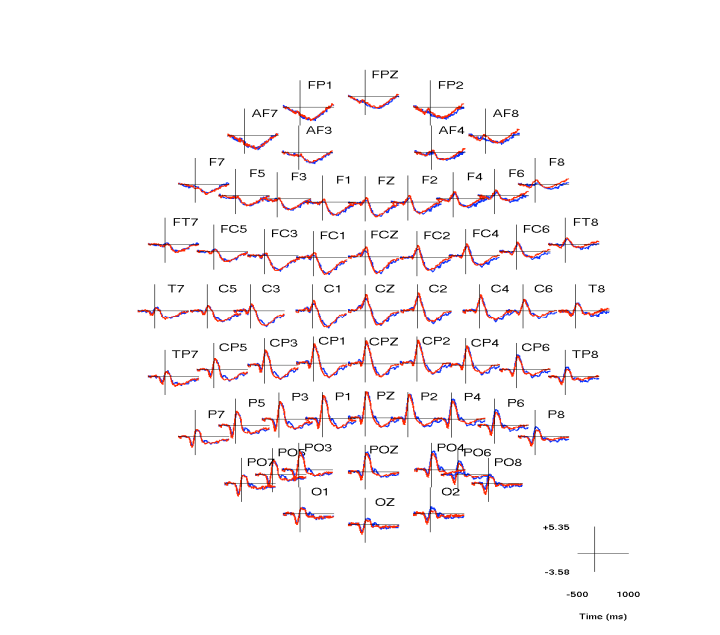

Grand average in the scalp array of leftward versus rightward movement trials of pre-processed EEG data for both (a) stimulus and (b) movement locking

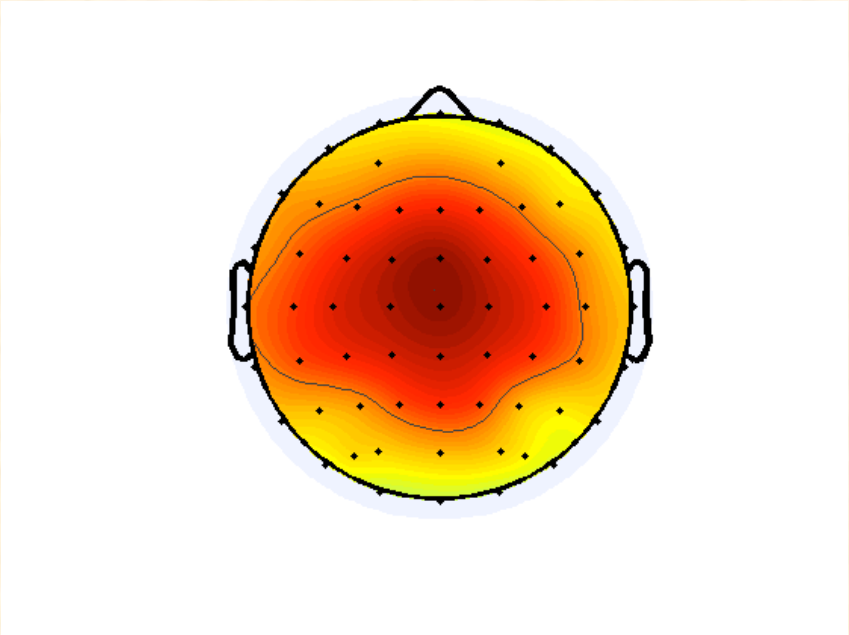

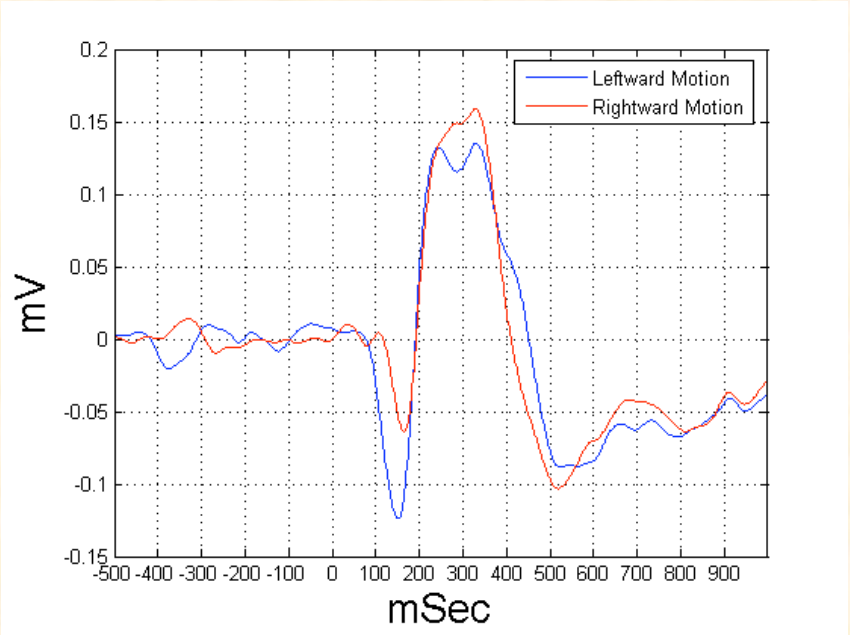

(a) The sensorimotor cortex weighted component average across subjects. (b) The corresponding grand average component activation for leftward versus rightward movement trials in the stimulus locked case. Rate: 74%, range 63-83%, $p \leq 0.0001$.

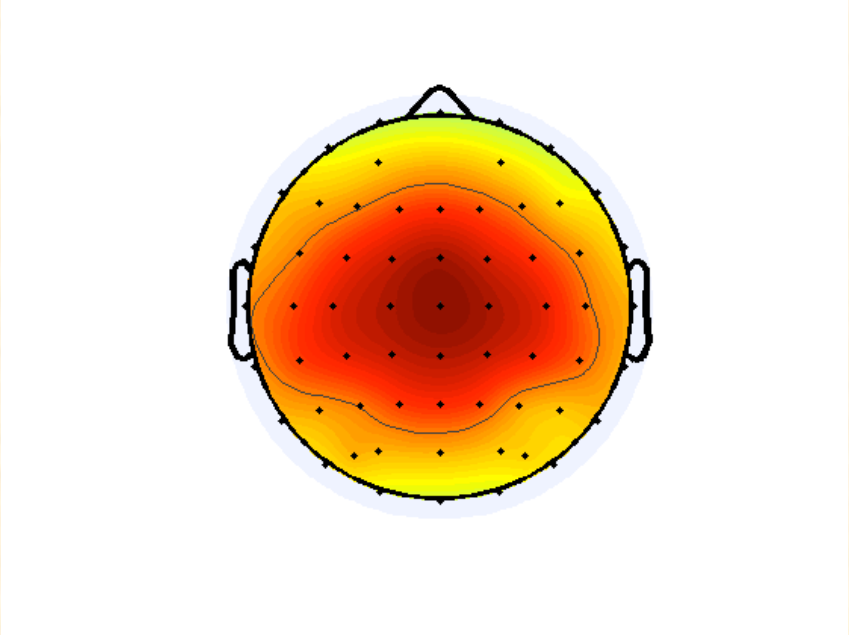

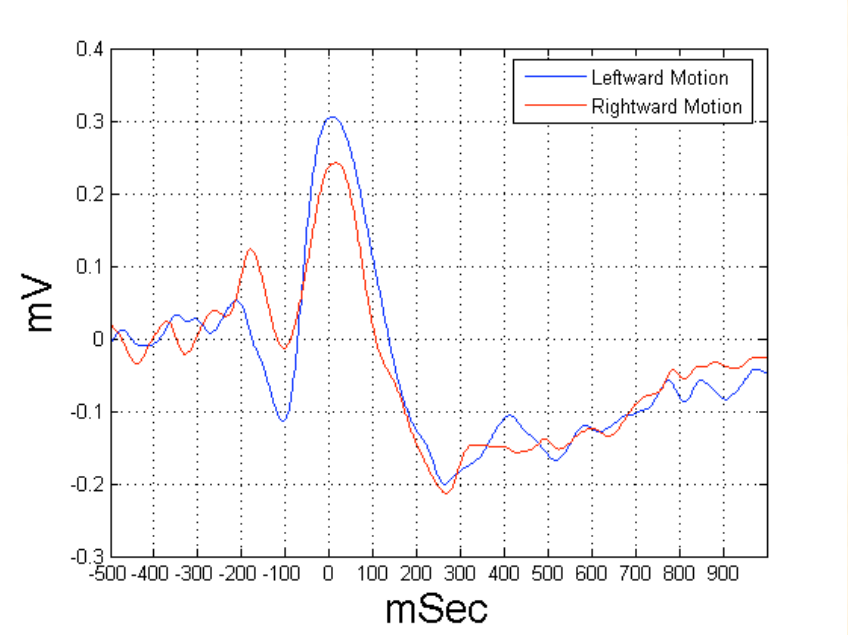

(a) The sensorimotor cortex weighted component average across subjects. (b) The corresponding grand average component activation for leftward versus rightward movement trials in the movement locked case. Rate: 72%, range 62-81%, $p \leq 0.0001$.